*Graphical Abstract

Internal structure and linear viscoelastic properties of EVA/asphalt nanocomposites

Markanday Subramanian Sureshkumar, Sara Filippi,, Giovanni Polacco,, Igor Kazatchkov, Jiri Stastna, and Ludovit Zanzotto

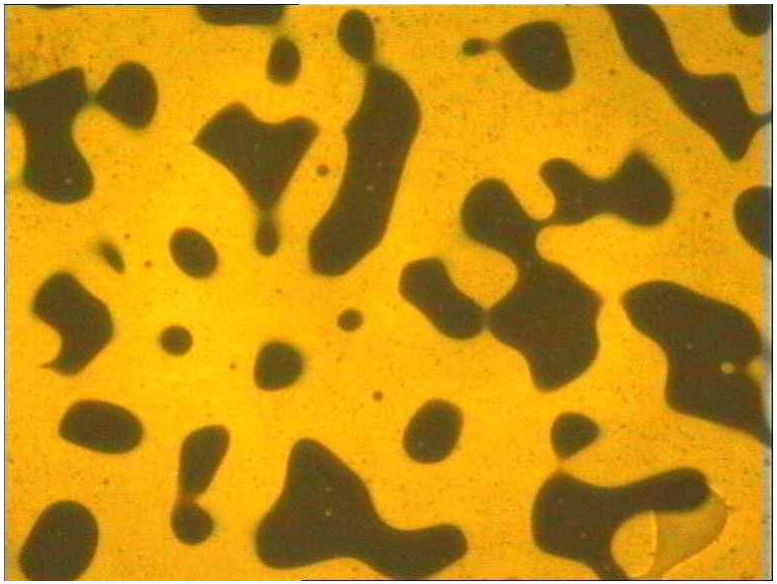

Internal structure and linear viscoelastic properties of EVA/asphalt nanocomposites

Markanday Subramanian Sureshkumar[a], Sara Filippi[a], Giovanni Polacco[a*],
Igor Kazatchkov[b], Jiri Stastna[b], and Ludovit Zanzotto[b]

[a]*Dipartimento di Ingegneria Chimica, Chimica Industriale e Scienza dei Materiali (DICCISM), Università di Pisa, Largo LucioLazzarino 2, 56122 –Pisa,Italy*
[b]*Bituminous Materials Chair, Schulich School of Engineering, University of Calgary, 2500 University Drive NW, Calgary, Alberta, T2N 1N4, CANADA*

Abstract

The effect of the addition of two different organoclays as a third component in polymer modified asphalts has been investigated. Ternary mixtures were prepared by adding clay and poly(ethylene-co-vinylacetate) to the asphalt, either separately, or in the form of a premixed master batch. The performed characterizations allowed the determination of how the two methods of mixing influence the interactions between asphalt and polymer and therefore the final rheological properties. In particular, it was shown that the clay had a compatibilizing effect on asphalt and polymer and that a high compatibility between clay and polymer led to a better dispersion of the polymer in the asphalt, thus influencing the final rheological properties of the studied systems.

Keywords

Polymer modified asphalt, EVA/organoclay, nanocomposites, rheology.

* Corresponding author: Tel: +39 050 2217820; Fax: +39 050 2217866

E-mail address: g.polacco@ing.unipi.it

Introduction

Asphalt is one of the oldest engineering materials and its existence dates back to around 1800 B.C. [1]. It was widely believed that, the term 'bitumen' originated in the ancient and sacred language of Hindus in India, Sanskrit [2]. Some of the historical names [3] are "esir" by Sumerians, "iddu" by Akkadians (which means that it comes from a place called "Hit"), "Sayali" or "Seyali" [4] or "zift" or "qar" by the Arabs of Iraq [2]. Forbes provides a detailed history of asphalt with a rare collection of pictures that support ancient application as a water proofing material [4]. In spite of this traditional application, today only about 10% of asphalt is used as roofing material, for thermal and acoustic insulation, humidity and corrosion protection components of paints and varnishes, etc., while the remaining 90% is used for paving. Asphalt binder constitutes only a small but crucial part of any paving mix. Thermo-mechanical properties of asphalt are determined by its complex internal structure that is not quite known, yet. Phenomenologically, asphalt can be characterized as a low molecular weight viscoelastic material with strong temperature susceptibility. At higher temperatures asphalt behaves as a viscoelastic liquid and at low temperatures it is a brittle viscoelastic material prone to cracking even at moderate loads. Moreover, at low temperatures asphalt can stay at non-equilibrium thermodynamic state for extended periods of time. This is the effect of its complex internal structure. Such a complex behavior creates problems in engineering applications of asphalt binder in paving mixes. Therefore, asphalt modification, with various types of materials, has been attempted to overcome, or at least delay, the above-described problems. Asphalt modification dates back many decades [2] and some of the modifiers are sulphur [5-7], carbon black [8], maleic anhydride [9], carboxylic acids [9], phosphazenes [10], lime [11], etc, but the most common modification is based on polymers and the term polymer modified asphalts (PMAs) refers to blends of asphalt and one or more polymers, usually added in percentages ranging from 3 to 7% by weight. Various kinds of polyolefins, natural rubber, thermoplastic elastomers, crumb rubber etc.

were investigated as modifiers of asphalt, but only a few were satisfactory from both the performance and cost points of view [12]. A list of polymers used for the modification of asphalt was reported by Isaccson [13].

Since the rediscovery of nano materials in 1985 at the Toyota Central R & D laboratory [14] and the subsequent development of polymer nanocomposites, such materials have generated a great deal of interest in the academic and industrial communities. Polymer nanocomposites basically consist of a blend of one (or more) polymer with various nanomaterials like nanoclays, carbon nanotubes, etc. Polymer-clay nanocomposites (layered silicate nanocomposites) are basically filled polymers in which at least one dimension of the dispersed phase is on a nanometer scale [15, 16]. Three types of structural arrangements are possible in layered silicate nanocomposites [17]: immiscible, where the polymer does not penetrate the bundle of silicate layers; intercalated, where the polymer chains penetrate the bundles of silicate layers without destroying the stacking layers; exfoliated (delaminated), where individual silicate layers are dispersed in the polymer. Polymer-clay nanocomposites are studied because of their superior thermo-mechanical properties even at low concentrations of clay [18]. Generally, the exfoliated nanocomposites (individual layers are irregularly delaminated and dispersed in a continuum polymer matrix) are materials with better physical properties when compared with intercalated nanocomposites [19]. Traditionally, the structure of nanocomposites is investigated by X-ray diffraction (XRD), transmission electron microscopy (TEM) and by differential scanning calorimetry (DSC) [15-18]. Lately, dynamic mechanical analysis (DMA) and other rheometric flows have been used in the study of nanocomposites. According to Krishnamoorti et al. [17], rheological studies showed a transition from liquid-like to solid-like behavior with little difference between intercalated and exfoliated nanocomposites. The time-temperature superposition principle was quite frequently used when studying the dynamic properties of nanocomposites [17, 18, 20]. Some examples of nanocomposite systems that

are not rheologically simple were given [20]. The creep study of polypropylene nanocomposites [21], showed a decrease of creep compliance, thus confirming the solid-like behavior of these systems. The ability of shear deformation, with large amplitudes, to orient nanocomposites was also studied [22-26]. In many cases the layered silicate nanocomposites behave like anisotropic materials i.e. the silicate layers orient in the shear direction. On the other hand some studies reported the perpendicular orientation of at least some fraction of silicate layers, [27-29]. Naturally the orientation of silicate layers will determine the properties of various material functions. When studying the polypropylene-clay nanocomposites by rheological methods it was shown that the effect of flow can lead to break down of the aggregate network, and possibly, the aligning of the structural elements [30]. This resulted in time and shear history dependence of rheological properties. Vermant et al [30], introduced a combination of transient flow protocols in order to separate the effects of flow on the aggregate structure and on the orientation of nanoclay domains. The degree of exfoliation was determined from the low frequency viscoelastic behavior and the high frequency behavior of dynamic moduli allowed estimation of the quality of dispersion.

From an engineering point of view an ideal asphalt binder should be resistant to permanent deformation at higher temperatures (in order to decrease the rutting potential of asphalt paving mixes), it has to be stable in storage and at low temperatures it should be less prone to the developments of cracks. The ultimate goal of modification of asphalt by polymers is to satisfy these requirements. Despite of many investigations these goals were not reached and moreover an unambiguous characterization of these systems is not known, yet. The use of ternary systems, asphalt/polymer/nanocomposite, is a novel approach to the asphalt modification and our intention was at first to study the properties of such individual systems before any suggestions can be made for practical use of these systems as binders in paving mixes. The present paper follows a previous one where the effect of the addition of clay as a

third component in polymer modified asphalt was investigated [31]. The main idea is, therefore, to combine the effects induced on the polymer properties by the addition of nanoclay, with the asphalt modification. The ternary blend can be defined as a polymer modified asphalt nanocomposite (PMAN). In the first paper [31], the asphalt was modified by using poly(styrene-butadiene-styrene) block copolymer (SBS). After a preliminary investigation on the binary asphalt/clay and polymer/clay blends, the ternary blends were prepared by adding the clay and polymer to asphalt, either separately or in the form of a premixed master batch. Intercalated nanocomposites with comparable interlayer distances and glass transition temperatures were obtained in both cases; however, the results showed that the mixing procedure significantly affected the final rheological properties. Here, a similar procedure is followed by using poly(ethylene-vinyl acetate) (EVA) as a main part of EVA-organoclay modifiers of a conventional asphalt.

EVA is a thermoplastic material, that resembles elastomers in softness and flexibility, which is commercially available with the percentage of vinyl acetate varying from 10 to 40 % depending on the requirements. After SBS, EVA is probably the most important polymeric modifier for asphalts and an abundant literature is already available, both for the virgin [32-35] and recycled [36-41] polymer. At the same time, EVA copolymers were intensively investigated for the preparation of nanocomposites [15, 17, 42-44]. For example, EVA nanocomposite [45] was prepared by melt intercalation with various concentrations of bentonite organoclay. The dynamic and steady shear material functions showed a remarkable difference when compared with those of pure EVA copolymer. It was also shown [45] that extensional viscosities were increasing with the content of silicate and strain hardening was observed. At higher strains, silicates have only a small effect on the extensional viscosities. In contrast with the behavior of pure EVA copolymer, systems with higher content of silicate showed a rapid shear thinning.

The thermal degradation and rheological properties of EVA-montmorillonite nanocomposites were studied by Riva et al. [44]. An increase of the storage and loss moduli was observed in nanocomposites when compared with those in pure EVA copolymer. At high temperatures, the difference between elastic moduli of various nanocomposites was also observed. The thermal behavior of EVA-layered silicate nanocomposites was studied by Zanetti et al. [43]. A slower thermal degradation and delayed weight loss were observed in these materials. Tensile properties of EVA-montmorillonite nanocomposites were investigated by Alexander et al. [42]. It was shown that Young's modulus increased significantly even at very low content of the filler while preserving high ultimate elongation and tensile stress. The shear and elongational flows of EVA-based nanocomposites were also studied in [46]. A stronger strain hardening was observed in nanocomposites when compared with the same effect in a pure EVA matrix. The impact of blending sequences on the microstructure and mechanical properties for ternary systems polypropylene/EVA/montmorillonite organoclay was discussed by Martins et al. [47]; they observed a relationship between the clay location and the morphology of ternary nanocomposites. A similar relationship was found between the morphology and mechanical properties of the studied systems. Moreover, electric insulation properties of EVA copolymer and EVA-layered silicate nanocomposites were studied by Gustavino et al. [48] where it was found that the presence of inorganic layered nanofillers improved the electric insulating properties.

EVA copolymer containing 28 wt % of vinyl acetate and two different types of nano clays were used to modify a base asphalt of penetration grade 50/70, thus preparing EVA/asphalt nanocomposites. After a preliminary study of the binary asphalt/clay and polymer/clay blends, the ternary blends were prepared by adding the clay and polymer to the asphalt, either separately or in the form of a premixed master batch. The obtained PMANs were found to have intercalated features in both cases. However, the results showed that the nature of the clay and the mixing procedure significantly affected the clay dispersion

and the blend morphology. This paper describes the thermo-mechanical, morphological and crystalline behavior of the prepared samples.

Materials and Methods

The base asphalt (BA) was 50/70 Pen grade conventional asphalt from vacuum distillation, with ring and ball softening point (RB) = 49 °C and penetration = 63 dmm. The polymer modifier was Greenflex HN70®, ethylene vinyl acetate copolymer with melt flow index 6 (190 ºC/10 min), containing 28 % of vinyl acetate with a shore A hardness = 75. Two different kinds of nano clays were utilized for the nano composite preparation. The first was Cloisite 20A®, (subsequently referred to as 20A) from Southern Clay Products, USA. 20A is an organoclay prepared from a sodium montmorillonite having a cation exchange capacity of 0.926 meq·g^{-1} by treatment with 0.95 meq·g^{-1} of $Me_2(HT)_2NH_4Cl$ (dimethyldihydrogenated-tallow ammonium chloride). Hydrogenated tallow is a blend of saturated n-alkyl groups with an approximate composition of C18 at 65%, C16 at 30% and C14 at 5%. The organic content of 20A was 38.5 wt% as determined by thermogravimetric analysis (TGA). The second nanoclay was Dellite 43B® (subsequently referred to as 43B), a clay derived from naturally occurring montmorillonite, especially purified and modified by dimethy dibenzyl hydrogenated from talloammonium, from Laviosa Chimica Mineraria, S.p.A., Livorno, Italy.

The polymer was carefully dried in a vacuum at 70°C, while both the asphalt and the organoclay were used as received from the suppliers.

Two sets of blends were prepared for each clay: 1) EVA/clay, 2) BA/EVA/clay. In all cases the weight ratio EVA/clay was set to 60/40. The EVA/clay blends were prepared by melt compounding in a Brabender Plasticorder static mixer of 50 mL capacity, preheated to 190°C (20A) or 120 °C (43B). The rotor speed was maintained at 30 rpm for about 2.5 minutes and then it was increased gradually (in 30

second increments) to 60 rpm. The organoclay was added into the molten polymer matrix before increasing the rotor speed. The overall blending time was 13 minutes. The applied torque and blend temperature were recorded during the whole compounding period. At the end, the molten products were extracted from the mixer and cooled naturally in the atmosphere. The blends were then made into sheets using a Carver Laboratory Press, Model C, Fred. S. Carver Inc., USA, at a temperature of 120 ºC. After cooling the sheets for 3 hours, they were cut into uniform chips.

A typical procedure for asphalt modification was as follows: aluminium cans of approximately 500 mL were filled with 250-260 grams of asphalt and put in a thermoelectric heater. When the asphalt temperature reached 180°C, a high shear mixer was dipped into the can and set to about 4,000 rpm. The polymer and clay (or the polymer/clay nanocomposite) were added gradually (5 grams per minute), while keeping the temperature within the range of 190±1°C during the addition and the subsequent 1.0 hour of mixing. Finally, the obtained PMA was split into appropriate amounts to prepare samples for the characterization. The samples were stored in a freezer at -20°C.

After preparation, the PMAs were characterized by the classical ring and ball softening point procedure (ASTM D36-76)) and by fluorescence microscopy (UNI prEN 13632).

Wide angle X-ray diffraction (WAXD) measurements were made in reflection mode with a Siemens D500 Krystalloflex 810 apparatus X-ray, with a wavelength of 0.1542 nm at a scan rate of 2.0 $°\cdot min^{-1}$. The clay was analyzed as a powder; and, the EVA/clay composites were analyzed as disks of 2 mm thickness and 20 mm diameter prepared by compression molding of the melt-compounded materials. The BA/clay and BA/EVA/clay samples were obtained directly from the mixing can and poured into small cylindrical moulds (10 mm diameter, 1 mm height), externally shaped to be directly allocated in the instrument.

Calorimetric analysis was carried out with a DSC Q100 differential scanning calorimeter from TA Instruments equipped with a modulated temperature set-up and a liquid nitrogen cooling system. Ultra pure nitrogen was used to purge the cell. Standard aluminum pans were used for all the experiments. The sample mass was in the range of 7-11 mg. The modulated DSC (MDSC) method for all asphalt samples was as follows: fast heating up to 150 ºC, isothermal for 5 min, cooling (10 ºC/min) to –60 ºC followed by a slower (2-4 ºC/min) cooling to –120 ºC, data were collected during heating with a rate of 4 ºC/min and an amplitude of ±3 °C every 40 s, until the sample reached 150 ºC. The MDSC data was used to determine the glass transition temperature, as well as the compatibility of the amorphous domain (through the derivative of reversing heat capacity). Standard differential scanning calorimetry (DSC) was performed upon cooling from 150 ºC to –120 ºC at 2 ºC/min for all samples. This test provided the onset temperature of crystallization and the enthalpy of crystallization.

Dynamic oscillatory measurements were performed (isothermal conditions) in small amplitude oscillatory shear flow, by using a TA ARES LS2-M rheometer, which operates under strain control. The geometries were the plate-plate (10, 25 and 50 mm diameters) and torsion bar (with linear dimensions of 37*12.5*2.7 mm) depending on the operating temperatures [49], which varied from -20 to +70 °C. The frequency was varied from 0.1 to 100 rad/s, depending on the temperature.

Asphalt samples were prepared by pouring the molten material into small cans in order to avoid frequent reheating and then loaded into the rheometer. This procedure assures that the morphology formed during the mixing stage is preserved until the rheological measurement is carried out. Preliminary strain sweep tests were performed in order to ensure that all experimental conditions remained in the linear domain. Master curves of the dynamic material functions (storage G’ and loss G” moduli, as well as the loss tangent tanδ) were built by applying the time-temperature superposition principle (Tr = 0°C) [50] with the help of the commercial software IRIS. The reference temperature of 0 °C was chosen because it was

about in the middle of the temperature interval of the individual testing temperatures. No anomalous behavior of these material functions was observed, the horizontal (a_T) shifting factors were easily fitted to the WLF form [50] and the applicability of the time-temperature superposition principle was verified for all the studied materials by constructing the van Gurp-Palmen [51] plots of the phase angle versus the magnitude of the complex modulus. Rheological properties of the materials discussed in this contribution are further described in [52] where the verification of rheological simplicity for all the studied materials can be found.

Results and discussion

As noted in the previous section, a first set of binary blends was prepared and characterized by X-ray analysis, in order to find out if, and what type of nanocomposites were formed when blending EVA and the two clays. Then, the ternary BA/EVA/clay mixtures were prepared by using a 60/40 (w/w) EVA/clay ratio and a content of 3 or 6% of polymer with respect to the total amount. Moreover, for each composition two ternary mixtures were prepared. The first one corresponded to physical mixing (PM) obtained by adding the polymer and clay separately to the asphalt during the modification, while the second one was obtained by adding the EVA/clay (60/40) nanocomposite as a master batch (MB). The total list of prepared asphalt mixtures is reported in Table 1, together with their respective softening points. The PMAs obtained with base asphalt and EVA are referred to as PMA3 and PMA6 depending on the polymer content. The PMANs are denoted as "polymer content/clay type/preparation method". As an example, 3/20A/MB is the ternary blend with 3% EVA and cloisite 20A from the master batch.

The softening point changed depending on the quantity of added polymer, and also on the type of nanoclay and preparation method. The addition of only EVA resulted in the increase of the "ring and

ball" temperature which was almost linear (4.5 °C for 3% and 10 °C for 6%) with the polymer content. In the presence of clay and physical mixing, there was a similar trend, but the ring and ball temperature increased a little more than in samples without clay. Analogously, the trend in EVA content remained qualitatively similar in the case of the MB mixtures, but a further increase in $T_{R\&B}$ was registered. This was true for both 20A and 43B, but cloisite seemed to have a slightly higher effect on the final performance. Therefore, the clay addition determined an increase in $T_{R\&B}$, which was clearly correlated with the addition method and this was a first indication that the PM and MB mixtures did have a different structure, at least with respect to the clay dispersion. We can suppose that i) in the case of MB the clay platelet remained confined in the polymeric phase whilst in PM there was stronger interaction with the asphalt phase, ii) cloisite could be dispersed better than dellite.

A further confirmation that the type of clay and the method of addition affected the structure of the mixtures was obtained from the morphological analysis (Figure 1). In all cases the mixtures with only 3% weight of added polymer were homogeneous, whilst significant differences were observed at higher polymer content. The binary mixture BA/EVA showed a two-phase morphology, with well-defined dark and white-grey areas. The dark zones corresponded to the asphalt rich phase whilst the grey part was the polymer rich phase, swelled by asphalt. In fact, this is a classical image consistent with the low compatibility between asphalt and polymer. More precisely, the polymer shows affinity with only some of the asphalt components and operates as a "local" solvent extraction agent where the most fluorescent components of asphalt (mainly the saturates and aromatics, which are less polar than resins and asphaltenes) migrated to the polymer phase, thus generating this two-color image. In the case of the 3/20A/PM mixture, the morphology appears to be qualitatively similar to that of the binary mixture, but the dimensions of the pattern are completely different. Moreover, the contrast between the dark and grey areas appears to be lower than in the binary mixture. This means that the clay enhances the

asphalt/polymer compatibility. The reason for this is probably the high polarity of the clay, which allows also the polar asphalt molecules to swell the polymer-rich phase. For the same reason, a better dispersion of the polymer was obtained in all the ternary mixtures, with clear difference between the morphology of the PM and MB samples. The most important difference that can be noted is the homogeneous aspect of the 6/20A/MB mixture. This result seems to suggest that in the MB mixture the clay has a better compatibilizing effect, than in PM. The reason could be the higher clay dispersion that can lead to a greater clay surface available for the interaction with asphalt molecules. Therefore, both the softening point and the morphological analysis suggest that cloisite leads to a better dispersion of EVA in the base asphalt.

These results are also confirmed by the XRD analysis. In Figure 2 the XRD traces of 20A and 43B clays and their EVA/clay 60/40 (w/w) master batches are reported. It is known from the literature [53, 54] that EVA copolymers, regardless of vinyl acetate content (9.3-40), give, by melt blending with little amount of 20A (1-7 wt %), intercalated/exfoliated nanocomposites, where the higher is the vinyl acetate content, the higher is the degree of exfoliation. Furthermore, Dubois and Coll [55] prepared two master batches EVA12/20A with 33 and 18 wt% of clay, observing that 20A intercalation is complete even at higher organosilicate content. According to these studies, we observed that the d_{001} peak of 20A clay (2θ = 3.5°, d = 2.5 nm) in the EVA/20A 60/40 XRD pattern (trace b) was shifted to a lower angle (2θ = 2.2°) corresponding to an interlayer spacing of about 3.9 nm. Therefore, all the tactoids were intercalated by EVA chains even at this very high organosilicate concentration. The clearly visible d_{002} and d_{003} orders also suggest the formation of intercalated tactoids with highly regular and coherent structure.

In the EVA/43B 60/40 XRD pattern (trace d) the original peak of 43B at about 4.8° was still present, but a new peak trace was observed at lower angle indicating that, in this case, we obtained only a partially intercalated hybrid, where the intercalation was not complete and some tactoids still remain unchanged.

This could be due to the high clay content but Li and Ha [56] found similar results preparing an EVA based nanocomposite using 3 wt% of Cloisite 10A, which was organomodified with the same ammonium cation as 43B. Similarly to Olabisi et al. [57], we also observed that the basal peak of the clay in the hybrid had a shoulder at higher angles. This probably means that part of the original tactoids that were not intercalated collapsed, perhaps due to degradation of the organo-modifier. With regard to the binary EVA/clay mixes, we can conclude that EVA/20A MB has a more homogeneous clay dispersion when compared with EVA/43B MB.

In Figure 3 the XRD patterns of BA/EVA/20A ternary mixtures prepared by PM (traces b and c) or by MB (traces d and e) are reported. The XRD analysis was performed on several different samples and it is important to underline that while for the mixtures prepared using the MB technique the data were consistent, when the mixtures were prepared by PM the intensity of the clay peak was highly scattered. This indicates that we obtained a more homogeneous dispersion of the clay using the master batch procedure than by adding the polymer and clay separately to the asphalt. For all the mixtures the basal spacing of the clay was shifted to the left with respect to the original position ($2\theta = 2.1$ °). With the interlayer spacing of about 4.1 nm, the results were quite similar to those obtained for the EVA/20A binary blend. For the mixtures prepared by master batches d_{002} and d_{003} peaks were also clearly defined as in the polymer nanocomposites. This probably means that the affinity of EVA and 20A is so high that the polymer chains remain in the gallery during the mixing with asphalt. Therefore, the highly polar clay probably acts as surfactant for the polymer in the asphalt matrix. In the physical mixtures, the tactoids have the same interlayer spacing but the higher orders are not clearly visible and the intercalated structure is not highly coherent. It is reasonable to assume that, by adding clay and EVA separately to the asphalt, the polymer chains were less efficient in intercalating the clay galleries because they compete with asphalt components and part of the polymer probably did not interact with the clay. In the

physical mixtures the surfactant action of the clay is therefore reduced and we can expect fewer homogeneous tactoids.

In Figure 4 the XRD patterns of BA/EVA/43B ternary mixtures prepared by PM (traces b and c) or by MB (traces d and e) are reported. For all the blends the original basal peak of the clay disappeared and was shifted to a lower angle, thereby indicating that asphalt can intercalate all the organosilicate galleries. The clay intercalation process of EVA/43B master batch was therefore completed by the asphalt components. Nevertheless, the d and e traces still showed a weak peak at higher angle (about 6°) corresponding to the collapsed tactoids formed during the EVA/43B MB preparation. For the same reasons as in BA/EVA/20A mixtures, we expect that the samples prepared by master batches should be more homogeneous with respect to those prepared by physical mixing. However the surfactant effect of 43B should be lower than that of 20A because this clay has less affinity for EVA and part of the polymer did not intercalate the clay.

MTDSC is capable of separating the overlapping thermal events via the decomposition of the total heat flow into the reversing and non-reversing components. Important information can be obtained from the derivative of the reversing heat capacity, dCp/dT, in the glass transition domain. By using this function one can study the multicomponent systems and their miscibility [57-59]. In a two component system of miscible blends, the function dCp/dT exhibited a single clear and symmetric peak. In physical mixtures this peak was broader, showing a shoulder or even another peak, depending on the difference between the glass transition temperature (Tg) of individual components. In the case of our systems, the situation was quite complex because asphalt itself, due to its colloidal structure and multicomponent nature, had an asymmetric peak with the maximum positioned at the glass transition temperature (Figure 5). Nevertheless, it is interesting to observe how this peak changed in shape when base asphalt was mixed with EVA (6% by weight) and clay. When BA was modified by EVA alone, the shoulder almost

disappeared, thus indicating that the polymer altered the internal structure of BA, and this can be associated with the already mentioned selective swelling of EVA by some of the asphalt components. In Figures 6 and 7, the graphs of dCp/dT are shown for systems with 6% EVA and the two clays. It can be seen that in the case of PM the shoulder is still visible and shifted to higher temperatures, while the curves for MB are similar to that of the binary asphalt/EVA mix. This seems to indicate that when polymer and clay are added separately there are different interactions between asphalt molecules and polymer. In PM samples, the asphalt had a weaker interaction with the polymer and maintained part of its original structure, while if the clay is dispersed (MB samples) in the polymer the latter remained able to absorb the asphalt molecules responsible for the shoulder. In systems with a low concentration of EVA (3% by weight) the effect of clays as well as the methods of preparation, on the shape of dCp/dT, was almost negligible.

With regard to the linear viscoelastic properties of the prepared samples, Figure 8 shows the master curves of *tan*δ as a function of the reduced frequency for all the PM mixtures. Two groups of curves can be easily identified: the first group is formed by the materials with 3 % content of EVA and the second one by the materials with 6% of EVA. In, Figure 9, the same material functions of the MB systems are shown.

The presence of nanoclay can be identified in both figures only at reduced frequencies ($\omega = a_T\ \tilde{\omega}$) less than 0.001 rad/s. The differences between the studied systems are more clearly seen on the graph of the modified loss tangent function (*tanc*(δ)=(J”-1/ωη$_o$)/J”, where J” is the loss compliance and η$_o$ is the zero-shear viscosity). This function represents the ratio of: (energy dissipated per cycle minus the energy dissipated due to the Newtonian flow) and (the energy stored and recovered per cycle). In all PMAN, the function *tanc*(δ) is a peak function that approaches zero at low, and high frequencies (corresponding to high and low temperatures). At low ω the graph of *tanc*(δ) is more steep than at high

ω where one can observe a rather long "tail". In 6% PMAN systems the maximum values of tanc(δ) were smaller than in 3% PMAN. This maximum was smallest for PMAN 6/20A/MB (Figure 10). The systems prepared by MB show a behavior quite different from those prepared by PM. In Figure 10 (MB) the function *tanc*(δ) shows a wide flat "peak" for systems with either clay. Such behavior was not observed in other PMAN systems studied in this contribution. From Figure 10 one can see that the system with clay 43B (melt blending method) started the Newtonian flow at much lower ω than the system with clay 20A (MB). In both of these materials the ratio of energy dissipated to the energy stored (assuming that the Newtonian flow is mainly carried by the base asphalt) in the clay-polymer matrix is only weakly dependent on the reduced frequency and this is true on a relatively large interval of ω (almost three orders of magnitude). Only for $\omega < 10^{-7}$ rad/s the flow begins in systems with clay 20A. The similar situation is observed for the system with clay 43B however, roughly at reduced frequencies less than 10^{-8} rad/s.

Thus the estimated zero shear viscosity of 6/43B/MB at 0°C was the highest of all the studied materials (Figure 11). This might mean less exfoliation, i.e. larger solid-like domains. In materials with clay 20A (the same method of preparation, MB), the zero shear viscosity is smaller and that might be due to better dispersion in this system. Generally, in modified systems, the zero shear viscosity and the steady state compliance increased when compared with the values of these parameters in the base asphalt, as expected. From a practical point of view, it means that modified systems became more stiff and more elastic, which might have a positive impact on low temperature cracking and high temperature rutting of pavements with such binders [60]. As an example, the discrete relaxation spectrum of 6/20A/MB is given in Figure 12. From this figure and also from Figure 9, it can be can seen that the performed dynamic testing covers the beginning of the terminal zone however, to cover the whole terminal zone

unreasonably high temperatures (rarely reached in pavements) would have to be used. Thus the values of the zero shear viscosity, given in Figure 11 have to be taken only as estimates.

Conclusions

The effect of clay addition as a third component in polymer-modified asphalts was investigated in a system composed of base asphalt, EVA copolymer and either an organomodified cloisite or dellite clays. The properties of the modified binders obtained with and without clay were compared. The ternary blends were prepared either by the separate additions of clay and polymer to the asphalt or by addition of premixed polymer/clay intercalated nanocomposites.

A simple morphological analysis showed that at high polymer concentrations the presence of the clay favors the dispersion of the polymer in the asphalt matrix. However, the two clays do not have the same effect and, moreover, also the method of clay addition is important. In particular, cloisite 20A, when premixed with EVA allowed obtain a completely homogeneous asphalt/polymer mixture at high polymer concentration. Thus the clay seems to have a compatibilizing effect in the asphalt/polymer interactions and cloisite is more efficient than dellite. A possible explanation of this effect can be attempted via the X-ray diffraction, which gave two main indications. The first one is that in the polymer/clay master batches, both clays have an intercalated structure, but cloisite appears to have a higher affinity with the polymer. In fact, cloisite is completely intercalated by the EVA chains; whilst with dellite a partially intercalated hybrid, containing unchanged tactoids, was obtained. The second indication is that some differences can be seen between the mixtures with analogous composition, but prepared by melt blending or physical mixing. Considering their chemical structure, it is easy to predict that clays have a higher affinity for asphalt than for the polymer. Therefore, in physical mixing the clays are mainly intercalated by the asphalt molecules. On the contrary, in the case of MB, the pre-formed

interactions between clay and polymer seem to survive the phase of mixing with asphalt. This is true for cloisite, but also for dellite, where the partial intercalation obtained with EVA is completed by the asphalt components. A qualitative confirmation of these findings is visible also in the MDSC traces where only in physical mixes the derivative of the reversing heat capacity shows a structure similar to that of the PMA.

Therefore, even if the clay is more compatible with asphalt than with polymer, once polymer/clay interactions are established, they are not altered by the asphalt molecules added subsequently. Moreover, the polymer/clay master batch, thanks to the clay, has a higher polarity than the polymer alone and this enhances the compatibility with asphalt. The clay acts as a surfactant that increases the interactions between the incompatible phases; the higher is the clay/polymer affinity, the higher is this effect. That is why the homogeneity in morphology increases going from asphalt/polymer to asphalt/polymer/dellite, to asphalt/polymer/cloisite.

The observed differences in the internal structure and polymer/clay dispersion, of course influence the rheology, which basically gave results coherent with the previous considerations. Moreover, the low values of the loss tangent function, in the studied system, indicate the better engineering properties of the material (higher elasticity, greater recovery i.e. smaller accumulated deformation during the repetitive loading etc.). Linear viscoelastic properties of the system were studied in this contribution and a deeper understanding of such complex systems can be achieved by studying also their nonlinear rheology. Preliminary investigations of nonlinear behavior of systems discussed here, are reported in [52].

Acknowledgements

The authors express their gratitude to the Natural Sciences and Engineering Research Council of Canada and to Husky Energy Inc. for their financial support of this work.

References

1 History of Bitumen, Nature 1935; 135 (3420): 845.

2 David W, John R. Shell bitumen handbook. In: Robert, H N, editor, Thomas Telford Ltd., 2003: p. 1-3

3 Zayan Bilkadii, Bitumen – A History, Saudi Aramco World 1984; 35(6): 2-9.

4 Forbes, RJ. Bitumen and Petroleum in Antiquity. In: Studies in Ancient Technologies, 2nd edn. Vol. 1, Leiden: E.J. Brill., 1964. p. 11-23.

5 Deme I. Processing of sand-asphalt-sulphur mixes. Proc. Ass. Asph. Pav. Tech., 1974; 43: 465-482.

6 Fromm, HJ and Kennepohl, G JA. Sulphur asphaltic concrete on three Ontario test roads. Proc. Ass. Asph. Pav. Tech., 1979; 48: 135-162.

7 Denning JH, Carswell J. Improvements in rolled asphalt surfacings by addition of organic polymers. Dept. Environ., Dept. Trans., Trans. and Road Res. Lab. Report, TRRL, Crowthorne, 1981; LR 989.

8 Chaala A, Roy C, Ait-Kadi, A. Rheological properties of bitumen modified with pyrolitic carbon black. Fuel 1996; 75(13): 1575-1583.

9 Herrington RR, Wu Y, Forbes MC. Rheological modification of bitument with maleic anhydiride and dicarbxylic acids. Fuel 1999; 78(1): 101-110.

10 Pokonova YuV, Mitrofanova LM. Modification of asphalts with phosphazenes, Chem Tech Fuels Oils 2005; 41(4): 315-318.

11 Shin-Che H, Rayond ER, Jan FB, Claine Petersen, J. Impact of lime modification of asphalt and freeze-thaw cycling on the asphalt-aggregate interaction and moisutre resistance to moisture damage. Jnl Mat Civ Eng 2005; 17(6): 711-718.

12 Polacco G, Stastna J, Biondi D, Zanzotto L. Relation Between Polymer Architecture and Nonlinear Viscoelastic Behavior of Modified Asphalts. Current Opinion in Colloid & Interface Science 2006; 11(4): 230-245.

13 Isaccson U, Lu X. Testing and appraisal of polymer modified road bitumens – state of art. Materials and Structures 1995; 28(3): 139-159.

14 Ray SS, Okamoto M. Polymer/layered silicate nanocomposites: a review from preparation to processing. Prog Polym Sci 2003; 28(11): 1539-1641.

15 Gupta RK, Pasanovic-Zujo V, Bhattacharya SN. Shear and extensional rheology of EVA/layered silicate-nanocomposites. Journal of Non-Newtonian Fluid Mechanics 2005; 128(2-3):116-125.

16 Alexander M, Dubois P. Polymer-layered silicate nanocomposites: preparation, properties and uses of a new class of materials. Materials Science and Engineering 2000; 28(1-2): 1-63.

17 Krishnamoorti R, Yurekli K. Rheology of polymer layered silicate nanocomposites. Current Oppinion in Colloid & Interface Science, 2001; 6(5-6): 464-470.

18 Chung JW, Han SJ, Kwak SY. Dynamic viscoelastic behavior and molecular mobility of acrylonitrile-butadiene copolymer nanocomposites with various organoclay loadings. Composite Science and Technology 2008; 68(6): 1555-1561.

19 Krishnamoorti R, Vaia RA, Giannelis EP. Structure and dynamics of polymer-layered silicate nanocomposites. Chem Mat 1996; 8(8) 1728-1734.

20 Zhao J, Morgan AB, Harris JD. Rheological characterization of polystyrene-clay nanocomposites to compare the degree of exfoliation and dispersion. Polymer 2005; 46(20): 8641-8660.

21 Galgali G, Ramesh C, Lele A. A rheological study on the kinetics of hybrid formation in polypropylene nanocomposites. Macrololecules 2001; 34(4): 852-858.

22 Krishnamoorti R, Silva AS. Rheological properties of polymer- layered silicate nanocomposites. In: Polymer-Clay Nanocomposites, Pinnavaia TJ, Beall GW, editors. Wiley, 2000. p.315-343.

23 Ren J, Silva AS, Krishnamoorti R. Linear viscoelasticity of disordered polystyrene-polyisoprene block copolymer based layered-silicate nanocomposites. Macromolecules 2000; 33(10): 3739-3746.

24 Krishnamoorti R, Ren J, Silva AS. Shear response of layered silicate nanocomposites. J Chem Phys 2001; 114(11): 4968-4973.

25 Kojima Y, Usuki A, Kawasumi M, Okada A, Kurauchi T, Kamigaito O, Kaji K. Novel preferred orientation in injection-molded nylon 6-clay hybrid. J Polym Sci B: Polym Phys 1995; 33(7): 1039-1045.

26 Kojima Y, Usuki A, Kawasumi M, Okada A, Kurauchi T, Kamigaito O, Kaji K. Fine structure of nylon 6-clay hybrid. J Polym Sci B: Polym Phys 1994; 32(4): 625-630.

27 Medelin-Rodriquez FJ, Burger C, Hsiao BS, Chu B, Vaia RA, Phillips, S. Time-resolved shear behavior of end-tetherd nylon 6-clay nanocomposites followed by non-isothermal crystallization. Polymer 2001; 42(2): 9015-9023.

28 Okamato M, Nam PH, Maiti P, Kotaka T, Hasegawa N, Usuki A. A house of cards structure in polypropylene/clay nanocomposites in elongational flow. Nano Letters 2001; 1(6): 295-298.

29 Schmidt G, Nakatani AL, Butler PD, Karim A, Han CC. Shear orientation of viscoelastic polymer-clay solutions probed by flow birefringence and SANS. Macromolecules 2000; 33(20): 7219-7222.

30 Vermant J, Ceccia S, Dolgovskij MK, Maffletone PL, Macosko CW. Quantifying dispersion of layered nanocomposites via melt rheology. J Rheol 2007; 51(3): 429-450.

31 Polacco G, Kříž P, Filippi S, Stastna J, D. Biondi D, Zanzotto L. Rheological Properties of Asphalt/SBS/Clay Blends. Euro Polym Jnl 2008; 44(11): 3512-3521.

32 Panda M, Mazumdar, M. Engineering properties of EVA modified paving mixes. J Mat Civ Eng 1996; 11(2): 131-137.

33 Airey GD. (2002). 'Rheological evaluation of EVA polymer modified bitumens. Con Build Mat 2002; 16(8): 473-487.

34 González O, Muñoz ME, Santamaría A, García-Morales M, Navarro FJ, Partal P. Rheology and stability of bitumen/EVA blends. Eur Poly J 2004; 40(10): 2365-2372.

35 Hussein IA, Iqbal MH, Al-Abdul-Wahab, HI. Influence of Mw of LDPE and vinyl acetate content of EVA on the rheology of polymer modified asphalts. Rheol Acta 2005; 45(1): 92-104.

36 García-Morales M, Partal P, Navarro FJ, Martinez-Boza F, Gallegos C, González O, González N, Muñoz ME. Viscous properties and microstructure of recycled EVA modified bitumen. Fuel 2003; 83(1): 31-38.

37 García-Morales M, Partal P, Navarro FJ, Martinez-Boza F, Gallegos C. Linear visco-elasticity of recycled EVA modified bitumen. Energy Fuels 2004; 18(2): 357-364.

38 García-Morales M, Partal P, Navarro FJ, Gallegos C. (2006). Effect of waste polymer additon on the rheology of modified bitumen. Fuel 2006; 85(7-8): 936-943.

39 García-Morales M, Partal P, Navarro FJ, Martinez-Boza F, Gallegos C. Process rheokinetics and micro-structure of recycled EVA/LDPE modified bitumen. Rheol Acta 2006; 45(4): 513-524.

40 García-Morales M, Partal P, Navarro FJ, Martinez-Boza F, Gallegos C. Processing, rheology and storage stability of recycled EVA/LDPE modified bitumen. Poly Eng Sci 2007; 47(2): 181-191.

41 González O, Muñoz ME, Santamaría A, García-Morales M, Navarro FJ, Partal P. New routes for roads: using recycled greenhouse films. Intl J Env Tech Mgmt 2007; 7(1-2): 218-227.

42 Alexander M, Beyer G, Henrist C, Cloots A, Ralmont R, Jerome R, Dubois P. Preparation and properties of layered silicate nanocomposites based on ethylene vinyl acetate copolymers. Macromol Rapid Commun 2001; 22(8): 643-646.

43 Zanetti M, Camino G, Thomann R, Mulhaupt R. Synthesis and thermal behavior of layered silicate EVA nanocomposites. Polymer 2001; 42(10): 4501-4507.

44 Riva A, Zanetti M, Braglia M, Camino G, Falqui L. Thermal degradation and rheological behavior of EVA/montmorillonite nanocomposites. Poly Deg Stab 2002; 77(2): 299-304.

45 Lee MH, Park BJ, Vhoi HJ, Gupta RK, Bhattachary SN. Preparation and rheological characteristics of ethylene-vinyl acetate copolymer/organoclay nanocomposites. J Macromol Sci:B Poly Phys 2007; 46(2): 261-273.

46 La Mantia FP, Tzankova Dintcheva N. EVA copolymer-based nanocomposites: Rheological behavior under shear and isothermal and non-isothermal elongational flow. Poly Test 2006; 25(5): 701-708.

47 Martins CG, Larocca NM, Paul DR, Pessan LA. Nanocomposites formed from polypropylene/EVA blends. Polymer 2009; 50(7): 1743-1754.

48 Gustavino F, Coletti G, Dardano A, Montanari GC, Deorsola F, Di Lorenzo Del Casale M. Electrical treeing in EVA-layered silicate nanocomposites. Annual Report Conference on Electrical Insulation and Dielectric Phenomena, 2005; 294-297.

49 Polacco G, Vacin OJ, Biondi D, Stastna J, Zanzotto L. Dynamic Master Curves of Polymer Modified Asphalt from Three Different Geometries. Applied Rheology 2003; 13(3):118-124.

50 Ferry JD. Viscoelastic Properties of Polymers. New York: Wiley; 1980.

51 Van Gurp M, Palmen J. Time-temperature superposition for polymeric blends. Rheol Bull 1998; 67: 5-8.

52 Markanday SS, Stastna J, Polacco G, Filippi S, Kazatchkov I, Zanzotto L. Rheology of Bitumen modified by EVA – organoclay nanocomposites. J Appl Polym Sci. submitted.

53 Lili Cui, Xiaoyan Ma, Paul DR. Morphology and properties of nanocomposites formed from ethylene-vinyl acetate copolymers and organoclays. Polymer 2007; 48(21):6325-6339.

54 Peeterbroeck S, Alexandre M, Jerome R, Dubois Ph. Poly(ethylene-co-vinyl acetate)/clay nanocomposites: Effect of clay nature and organic modifiers on morphology,mechanical and thermal properties. Polym Degrad Stab 2005; 90(2): 288-294.

55 Mainil M, Alexandre M, Monteverde F, Dubois P. Polyethylene organo-clay nanocomposites: the role of the interface chemistry on the extent of clay intercalation/exfoliation. J Nanosci Nanotech 2006; 6(2): 337-344.

56 Li X, Ha CS. Nanostructure of EVA/organoclay nanocomposites: effects of kinds of organoclays and grafting of maleic anhydride onto EVA. J Appl Polym Sci 2003; 87(12): 1901-1909.

57 Olabisi O, Robeson L, Shaw MT. Polymer-Polymer Miscibility In: Polymer-Polymer Compatibiliy. New York:Academic Press, 1979.

58 Song M, Hammiche A, Pollock HM, Hourston DJ, Reading M. Modulated differential scanning calormetry: 4. Miscibility and glass transition behaviour in poly(methyl methacrylate) and poly(epichlorohydrin) blends. Polymer 1996; 37(25): 5661-5665.

59 Song M, Hammiche A, Pollock HM, Hourston DJ, Reading M. Modulated differential scanning calorimetry: 1. A study of the glass transition behaviour of blends of poly(methy methacrylate) and poly(styrene co-acrylonitrile). Polymer 1995; 36(17): 3313-3316.

60 Michalica P, Kazatchkov IB, Stastna J, Zanzotto L. Relationship between chemical and rheological properties of two asphalts of different origins. Fuel 2008; 87(15-16): 3247-3253.

Figure captions

Figure 1 – Fluorescence microscopy of the produced mixtures.

Figure 2 – XRD patterns of: (a) 20A, (b) 20A/MB, (c) 43B, (d) 43B/MB.

Figure 3 – XRD patterns of: (a) BA, (b) 3/20A/PM, (c) 6/20A/PM, (d) 3/20A/MB, (e) 6/20A/MB.

Figure 4 – XRD patterns of: (a) BA, (b) 3/43B/PM, (c) 6/43B/PM, (d) 3/43B/MB, (e) 6/43B/MB.

Figure 5 – Derivative of the reversing heat capacity for BA, PMA3 and PMA6.

Figure 6 – Derivative of the reversing heat capacity for PMA6, 6/43B/PM and 6/43B/MB.

Figure 7 – Derivative of the reversing heat capacity for PMA6, 6/20A/PM and 6/20A/MB.

Figure 8 – Master curves of tanδ for PMA3, PMA6 and mixtures prepared by PM.

Figure 9 – Master curves of tanδ for PMA3, PMA6 and mixtures prepared by MB.

Figure 10 – Master curves of tancδ for PMA6, 6/43B/MB and 6/20A/MB.

Figure 11 – Estimates of the zero shear viscosity at 0 °C for all the studied systems.

Figure 12 – Discrete relaxation spectrum of 6/20A/MB.

Table 1 – Prepared mixtures.

Mixture	EVA (wt. %)	20A (wt. %)	43B (wt. %)	Prep. Method	$T_{R\&B}$ (°C)
BA					**49**
PMA3	**3**	**-**	**-**	**-**	**53**
3/20A/PM	**3**	**2**	**-**	**PM**	**55**
3/20A/MB	**3**	**2**	**-**	**MB**	**57.5**
3/43B/PM	**3**	**-**	**2**	**PM**	**54**
3/43B/MB	**3**	**-**	**2**	**MB**	**55**
PMA6	**6**	**-**	**-**	**-**	**59**
6/20A/PM	**6**	**4**	**-**	**PM**	**61.5**
6/20A/MB	**6**	**4**	**-**	**MB**	**65.5**
6/43B/PM	**6**	**-**	**4**	**PM**	**59.5**
6/43B/MB	**6**	**-**	**4**	**MB**	**64**

Figure(s)

Click here to download high resolution image

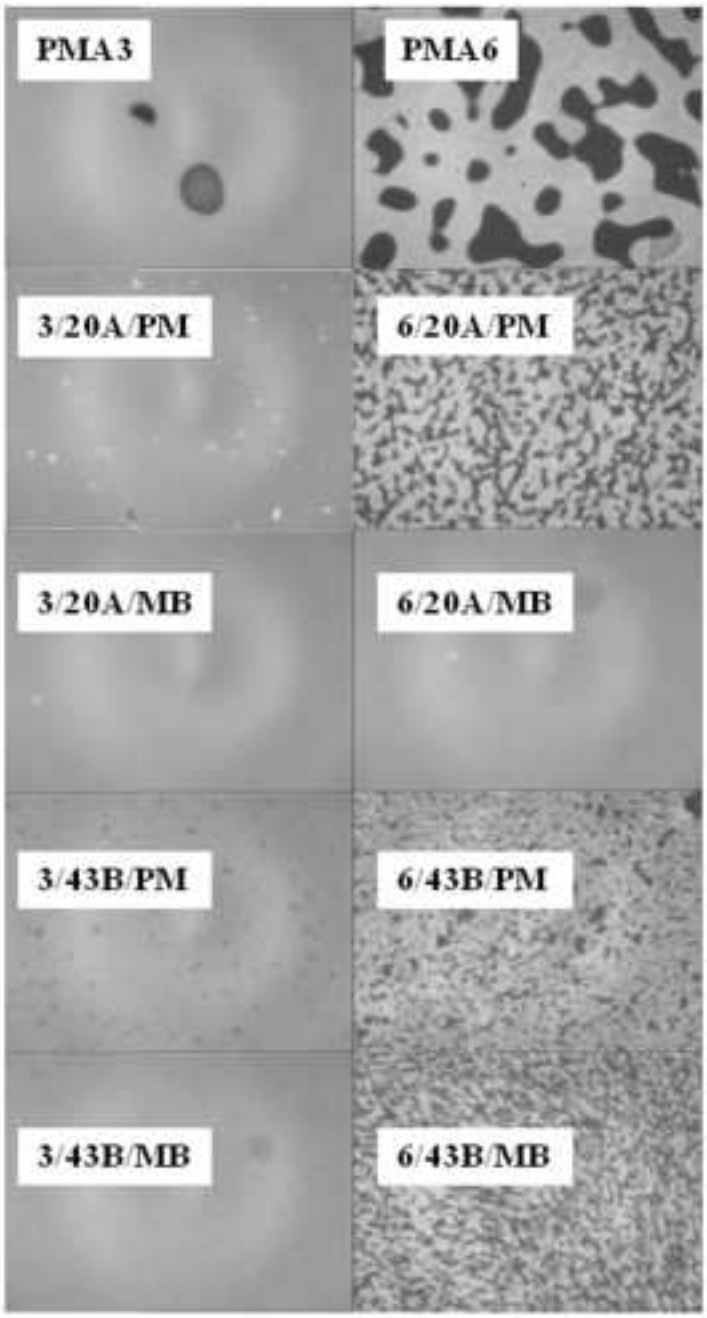

Figure(s)

Click here to download high resolution image

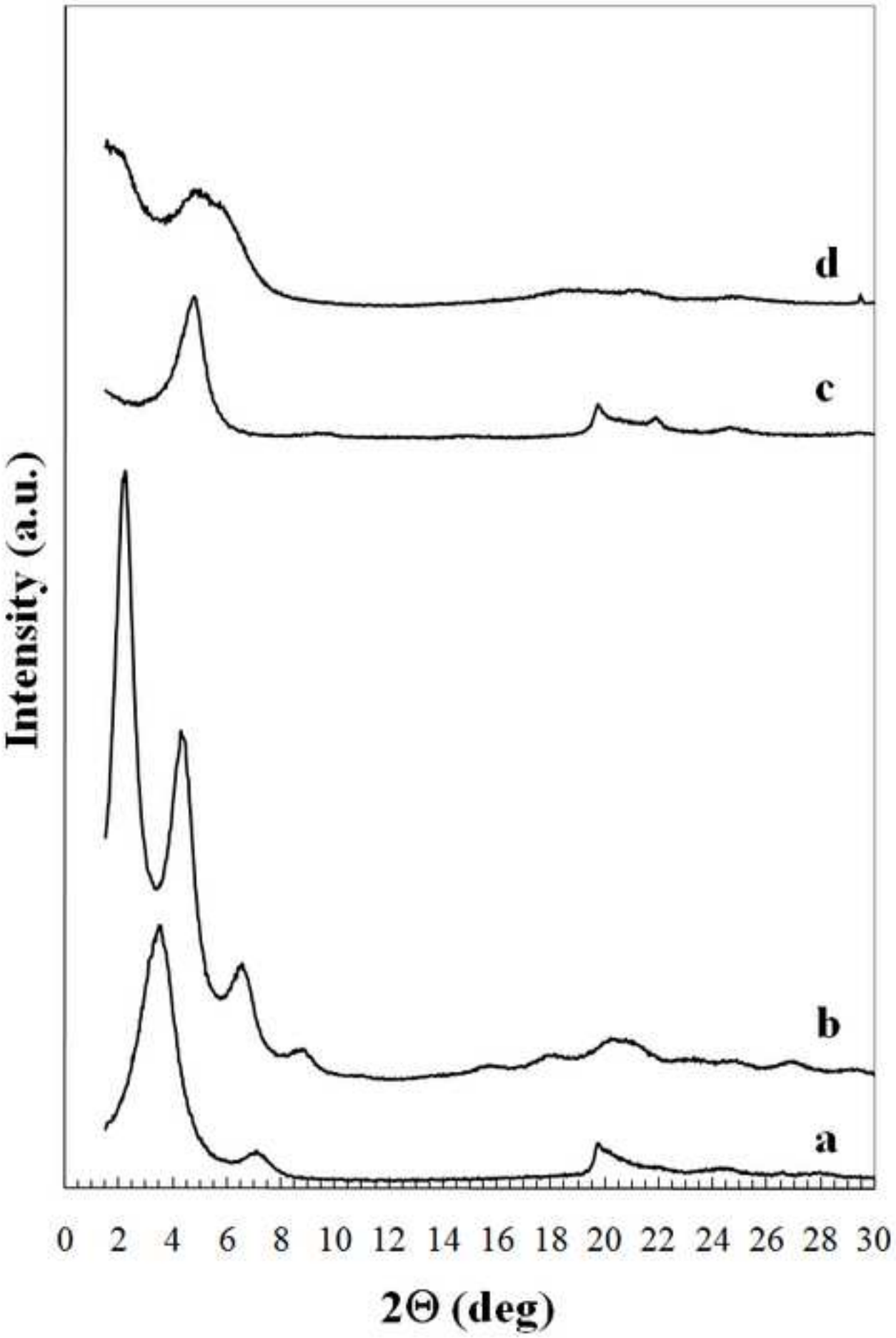

Figure(s)

Click here to download high resolution image

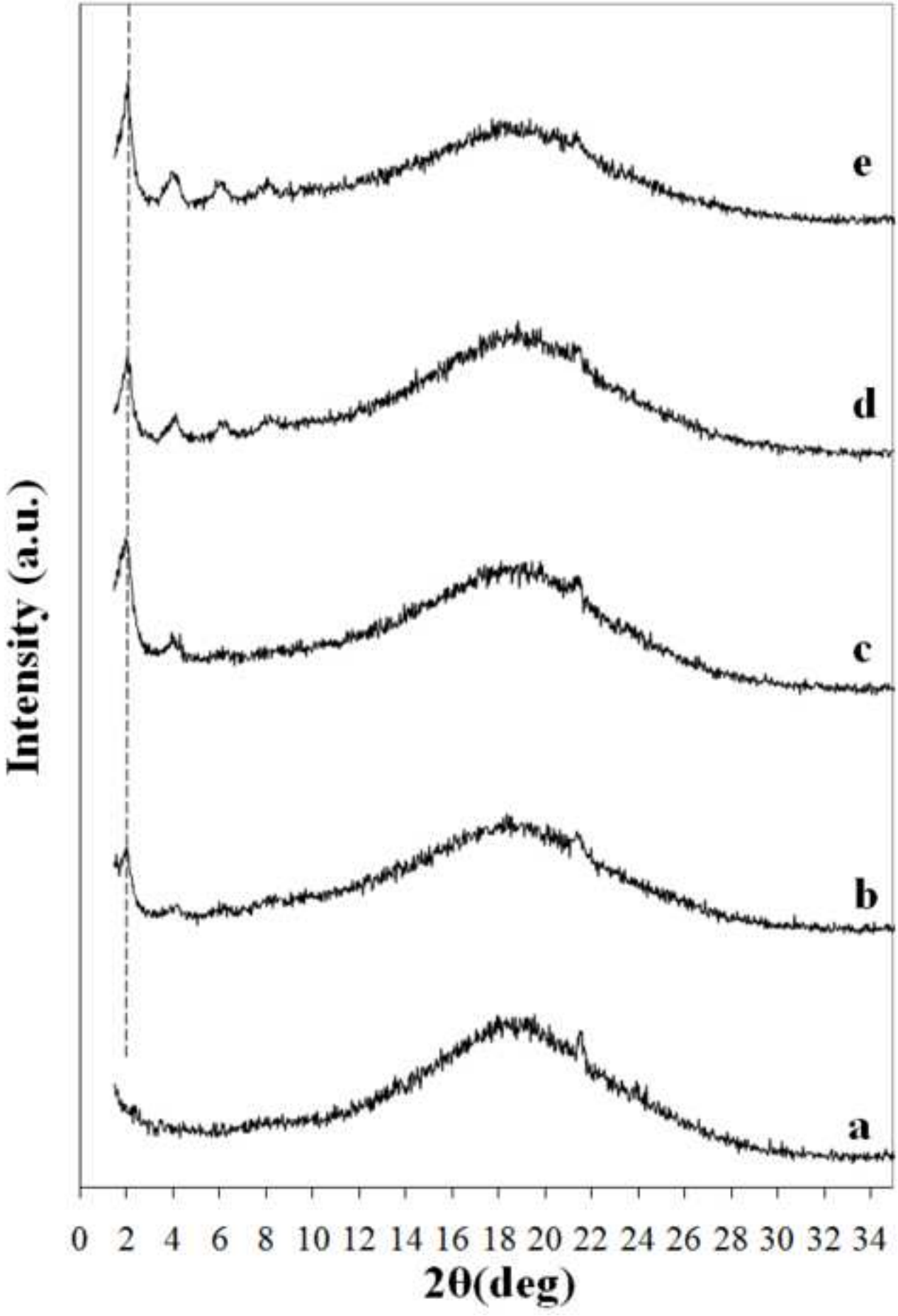

Figure(s)

Click here to download high resolution image

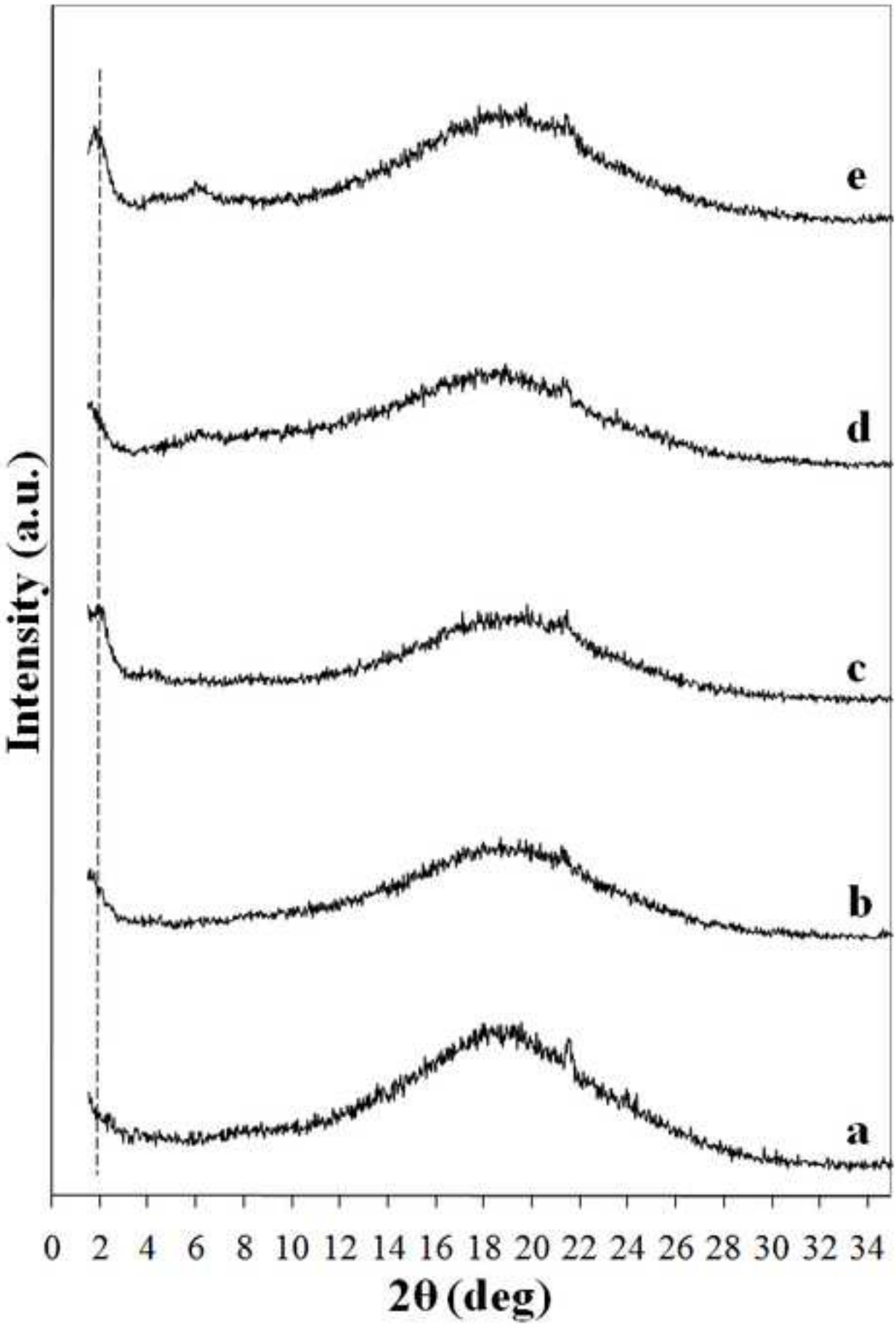

Figure(s)

Click here to download high resolution image

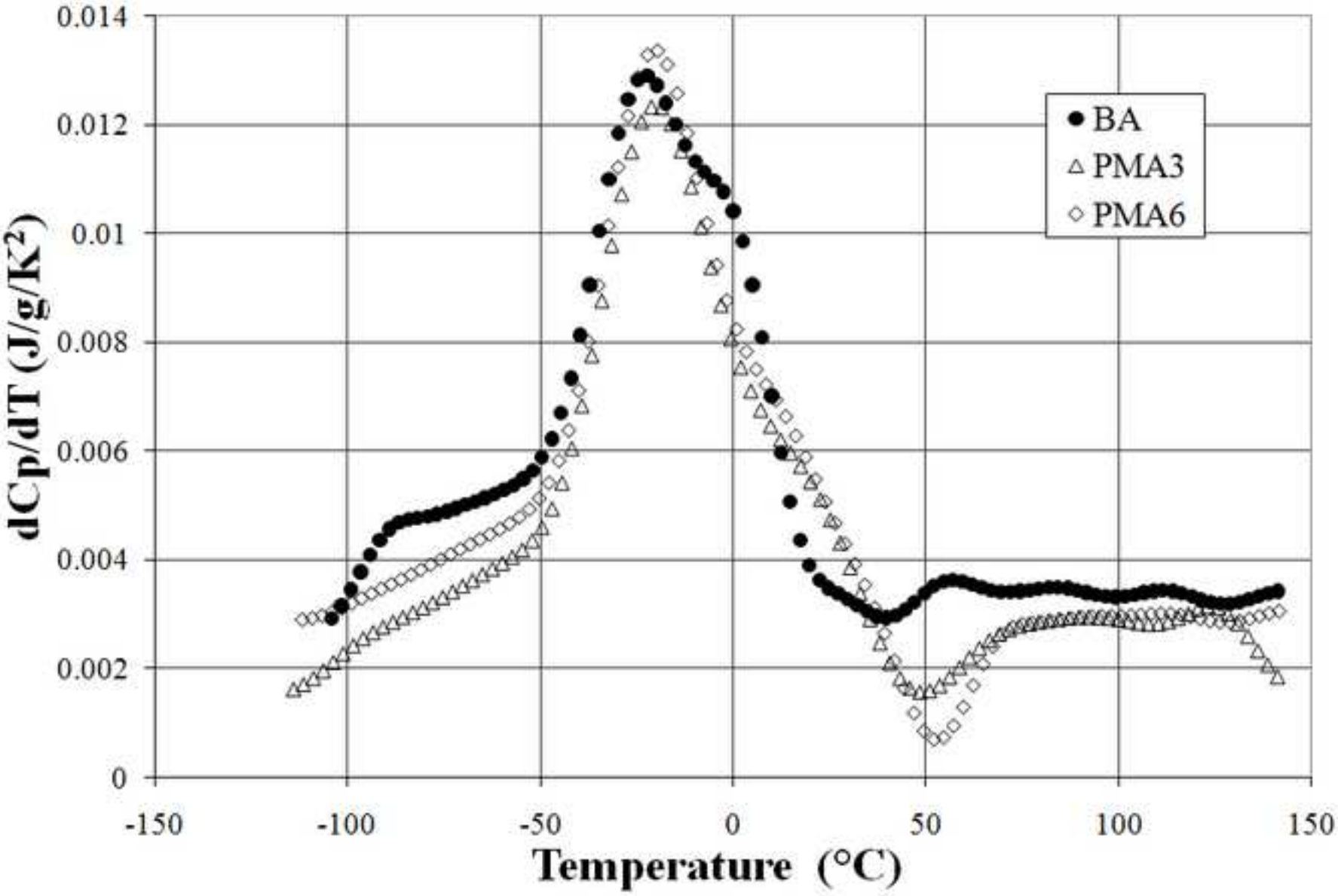

Figure(s)

Click here to download high resolution image

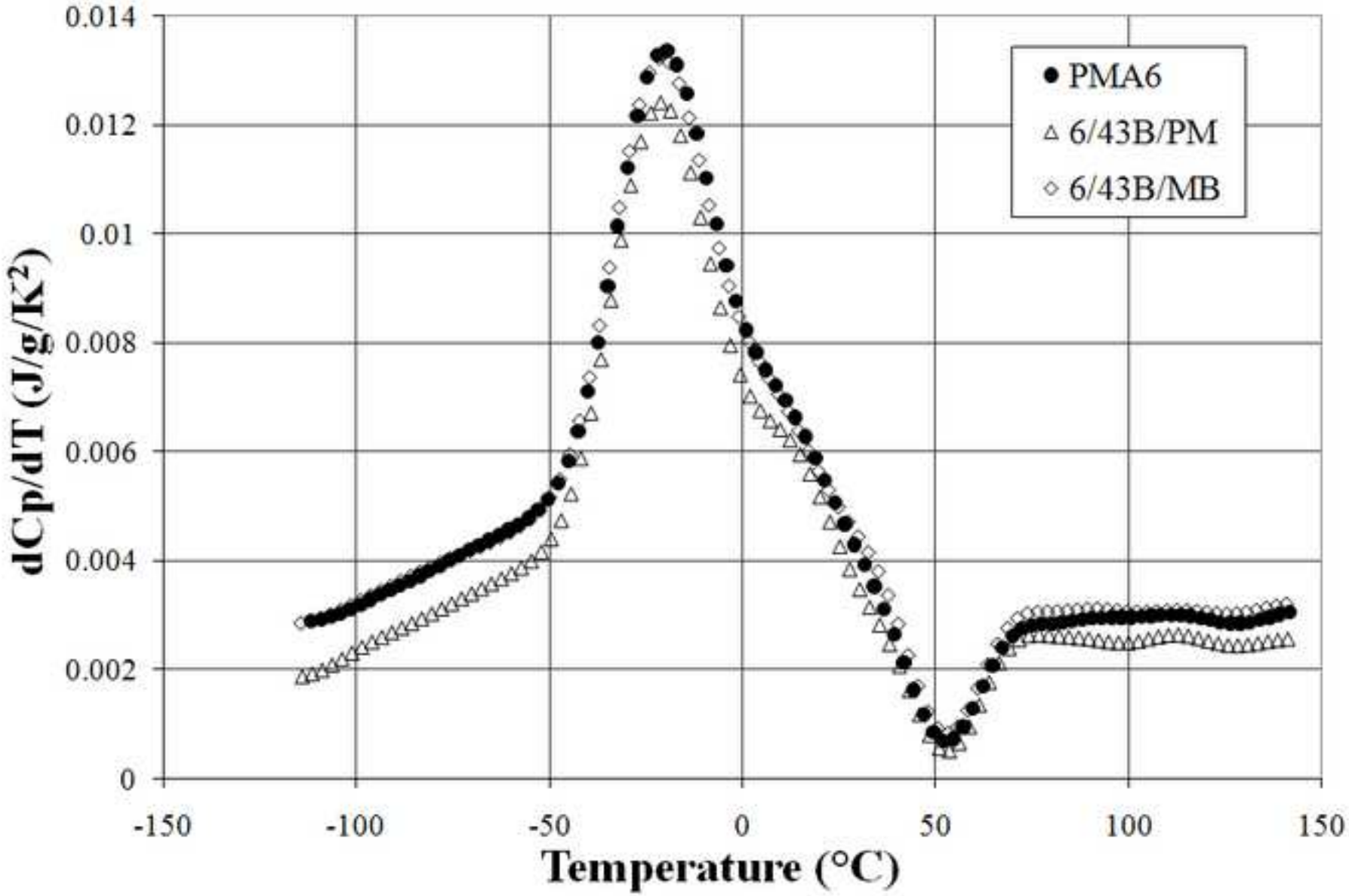

Figure(s)

Click here to download high resolution image

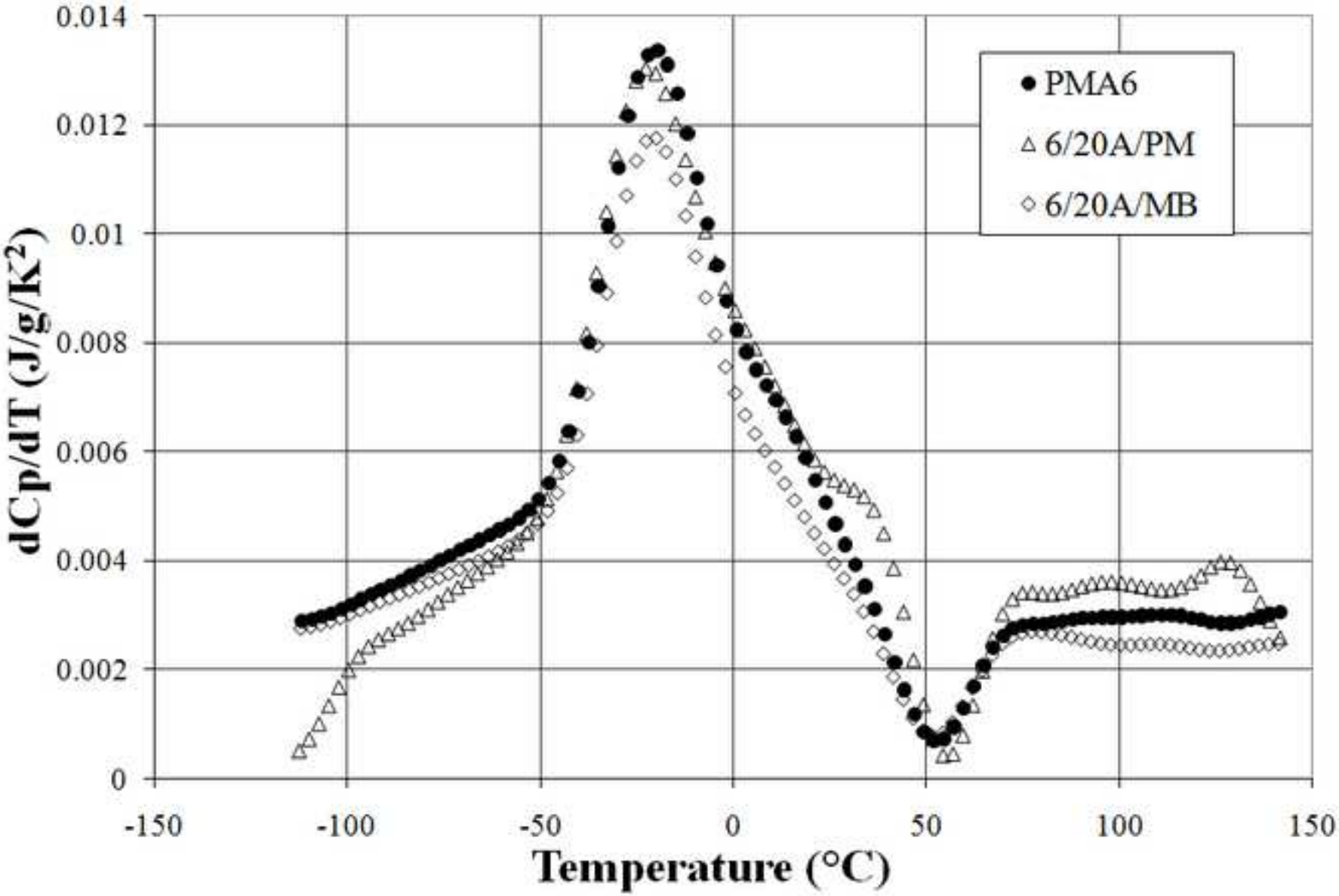

Figure(s)

Click here to download high resolution image

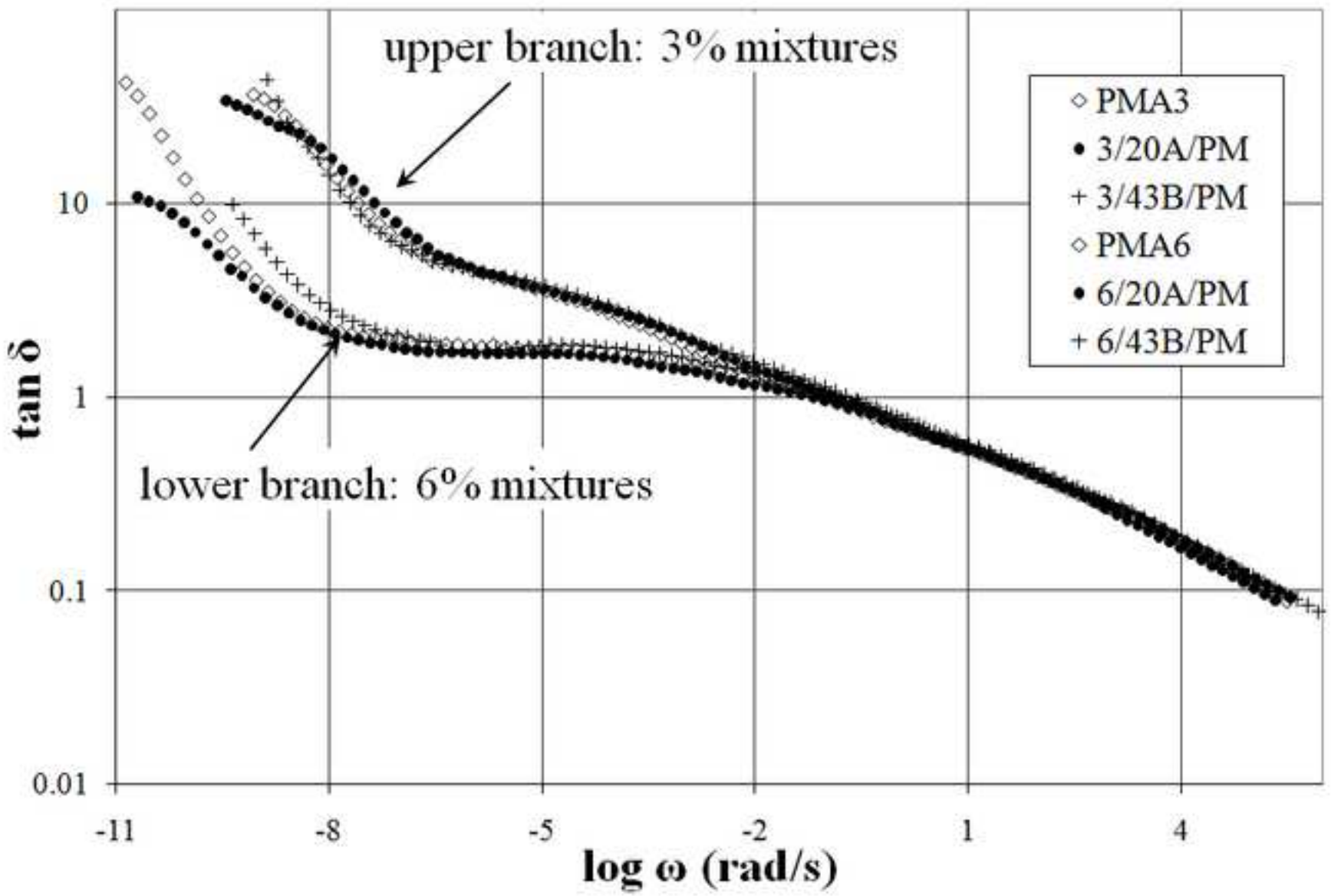

Figure(s)
Click here to download high resolution image

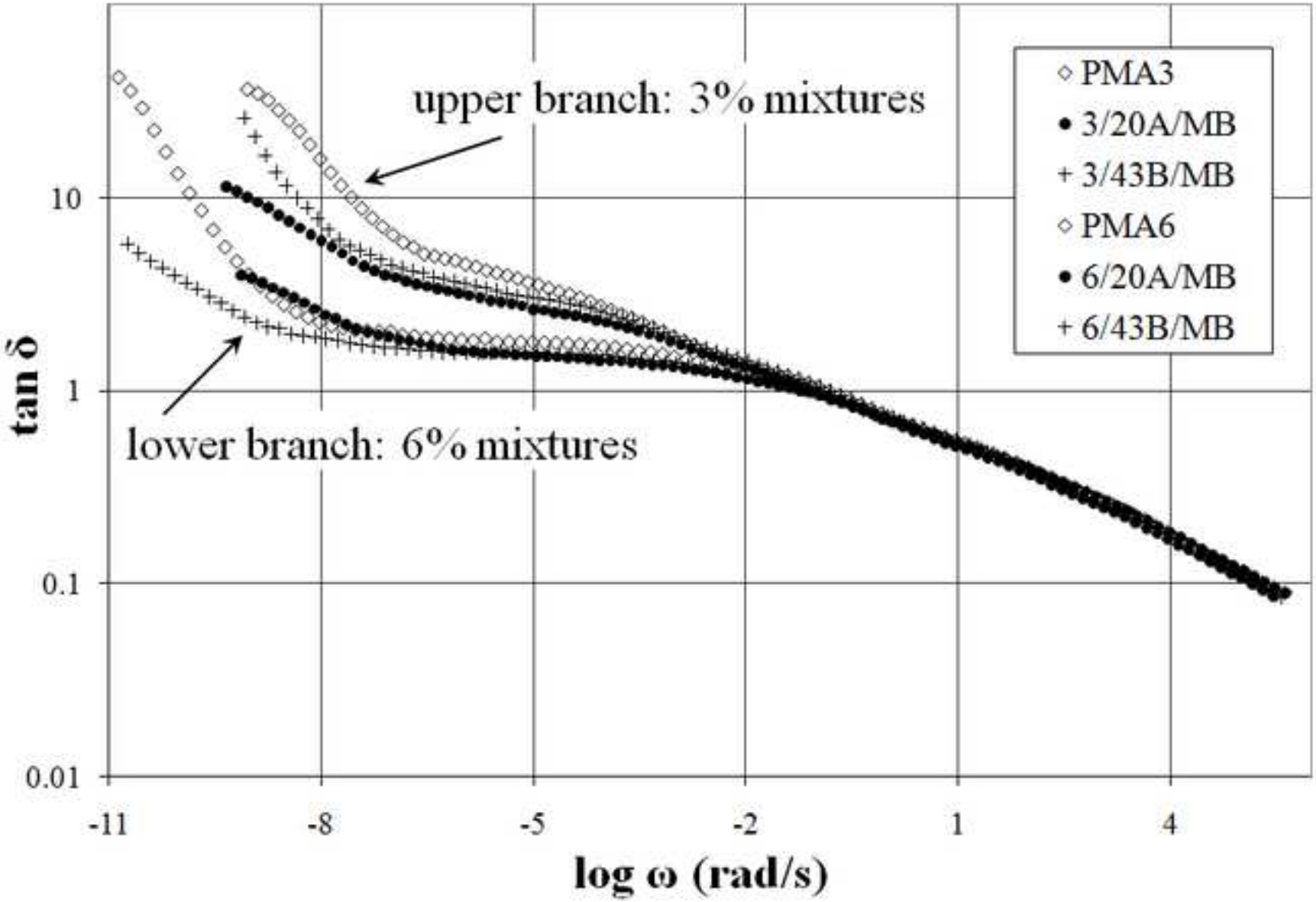

Figure(s)
Click here to download high resolution image

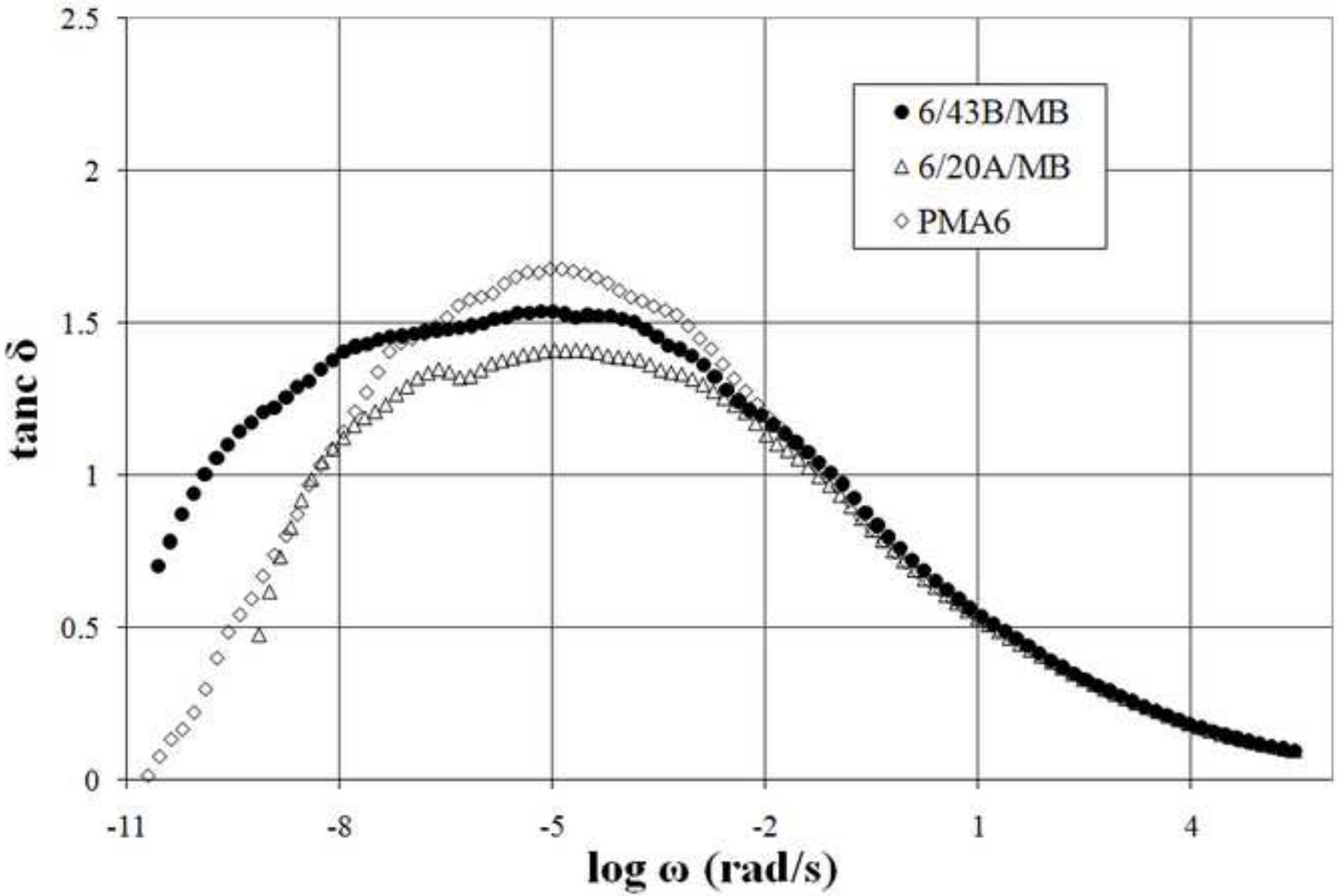

Figure(s)

Click here to download high resolution image

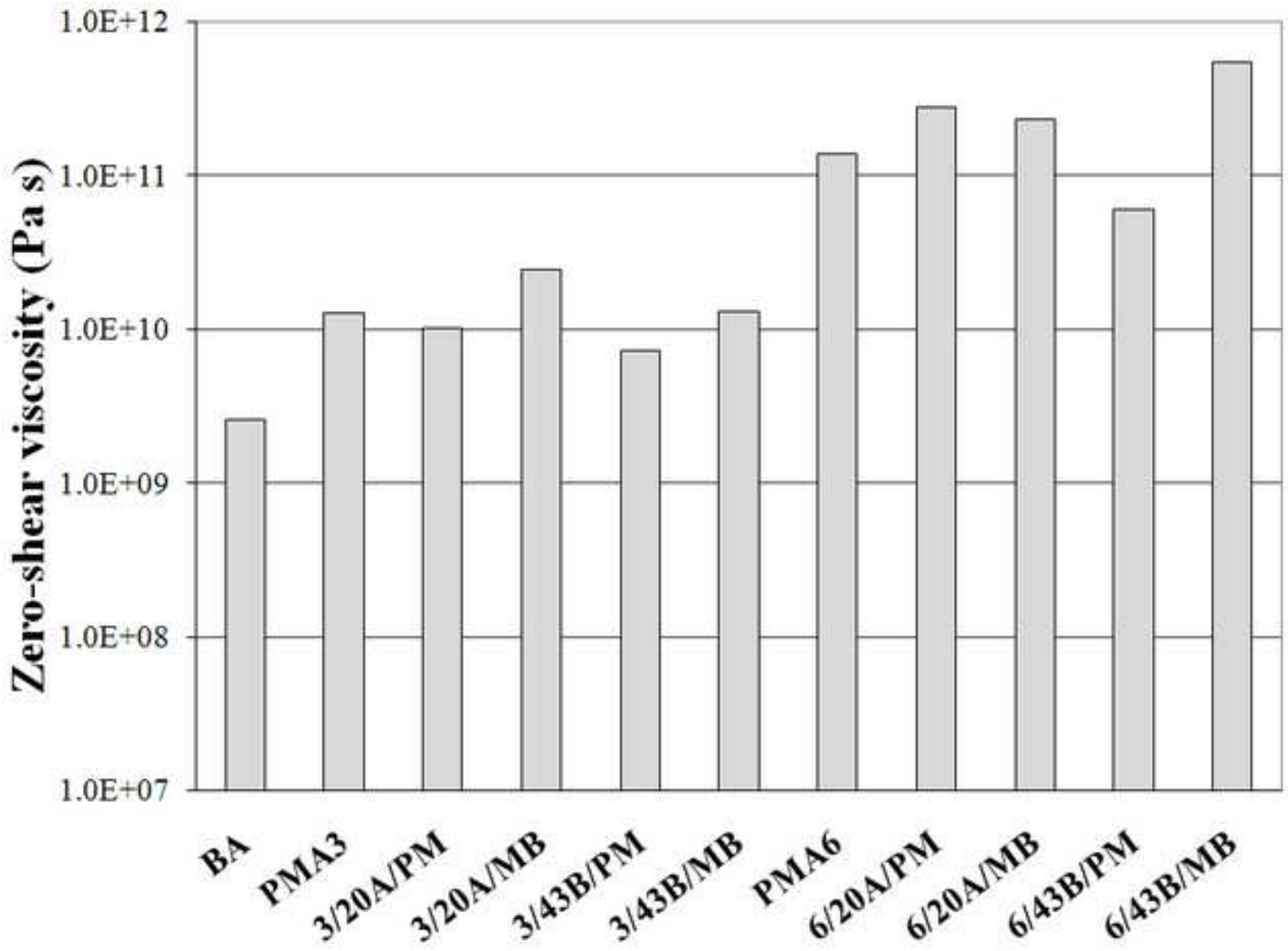

Figure(s)

Click here to download high resolution image